J. Chem. Sci. (2020)132:137
https://doi.org/10.1007/s12039-020-01826-w

REGULAR ARTICLE

Role of supramolecular interactions in crystal packing of Strandberg-type cluster-based hybrid solids

JISHA JOSEPH[a], CINU WINSON[a], BHARTI SINGH[b], JEMINI JOSE[c] and JENCY THOMAS[a,*]
[a]Centre for Sustainability Science, Research & PG Department of Chemistry, St. Thomas College (Autonomous), Thrissur, Kerala 680 001, India
[b]Department of Chemistry, Indian Institute of Technology Delhi, Hauz Khas, New Delhi 110 016, India
[c]Department of Chemistry, CHRIST (Deemed to be University), Bengaluru 560 029, India
E-mail: jencythomas@stthomas.ac.in

MS received 5 May 2020; revised 2 July 2020; accepted 9 July 2020

Abstract. Two new Strandberg-type cluster-based phosphomolybdates {H-2*a*3*mp*}$_5$[{PO_3(OH)}{PO_4}-Mo_5O_{15}], **1** and {H-2*a*4*mp*}$_5$[{PO_3(OH)}{PO_4}Mo_5O_{15}]·6H_2O, **2** have been crystallized *via* solvent evaporation technique using 2-amino-3-methylpyridine (2*a*3*mp*) and 2-amino-4-methylpyridine (2*a*4*mp*) respectively. The solids were characterized using single-crystal X-ray diffraction, powder X-ray diffraction, fourier transform infrared spectroscopy, thermogravimetric analysis, scanning electron microscopy and cyclic voltammetry. The solid **1** crystallized in monoclinic system with space group $P2_1/c$, a = 8.394(1), b = 27.398(6), c = 21.521(4) Å, β = 97.68(3)°, Z = 4. The solid **2** crystallized in triclinic system with space group P-1, a = 11.728(1), b = 14.234(1), c = 19.589(1) Å, α = 68.906(3), β = 89.454(3), γ = 66.559(3)°, Z = 2. The solids **1** and **2** formed a supramolecular framework stabilized by hydrogen bonding interaction between cluster anions and organic moieties. CH…π interactions between the organic moieties reinforced the crystal packing in **1** and **2**. While crystal packing effects resulted in the formation of solvent-accessible voids in **1**; aggregation of lattice water molecules in **2** facilitated the formation of pentameric water cluster. In addition, electrochemical behavior of **1** and **2** has also been investigated.

Keywords. Phosphomolybdate; Strandberg-type; supramolecular interactions; electrochemical behavior.

1. Introduction

Supramolecular assemblies based on phosphomolybdate (PMO) cluster anions are captivating organic-inorganic hybrid solids on account of their diverse topologies, tunable size and structural versatility.[1,2] Owing to their unique structural features, they exhibit a wide range of applications in multiple areas such as catalysis,[3,4] magnetism,[5] ion-exchange[6,7] and electrochemistry.[8–10] Among the PMO cluster anions, Strandberg-type $\{P_2Mo_5O_{23}\}^{6-}$ (abbreviated as $\{P_2Mo_5\}$ henceforth) is the most stable cluster anion that can be crystallized under ambient conditions.[11–13] It was first reported by Strandberg in 1973[14] and so far several hybrid solids have been reported based on $\{P_2Mo_5\}$ cluster anion with promising properties.[15–18] Majority of these solids have been crystallized along with protonated organic ligands having nitrogen donor atoms.[19–21] Since $\{P_2Mo_5\}$ cluster anion is stable in the pH range 1-7, organic ligands tend to be protonated (at pH < pK_a) and electrostatic interaction between the organic cations and inorganic polyanions enables the crystallization of hybrid solids. The protonated ligands exhibit hydrogen bonding interactions along with CH…π and/or π…π interactions which lead to the stabilization of the supramolecular aggregates and result in fascinating 3-D networks.[22–24]

For the past decade, our group has been investigating the role of supramolecular interactions in stabilizing the crystal packing in $\{P_2Mo_5\}$ cluster-based solids.[25–28] It was observed that these solids demonstrate remarkable structural characteristics such as porosity, aggregation

*For correspondence

Electronic supplementary material: The online version of this article (https://doi.org/10.1007/s12039-020-01826-w) contains supplementary material, which is available to authorized users.

Published online: 07 October 2020

of water clusters and supramolecular isomerism.[28,29] However, the electrochemical behavior of Strandberg-type cluster-based solids is proportionately less investigated. Therefore, in the present work, an attempt has been made to crystallize hybrid solids based on Strandberg-type $\{P_2Mo_5\}$ cluster, examine the role of supramolecular interactions in stabilizing the crystal packing in the solids and explore the electrochemical nature of the synthesized solids. Under ambient temperature, $\{H\text{-}2a3mp\}_5[\{PO_3(OH)\}\{PO_4\}Mo_5O_{15}]$, **1** and $\{H\text{-}2a4mp\}_5[\{PO_3(OH)\}\{PO_4\}Mo_5O_{15}]\cdot 6H_2O$, **2** were crystallized from an aqueous medium using isomeric ligands *viz.* 2-amino-3-methylpyridine (*2a3mp*) and 2-amino-4-methylpyridine (*2a4mp*) respectively through solvent evaporation technique. A detailed structural analysis of the solids revealed the role of H-bonding and CH… π interactions in the self-assembly of **1** and **2**. Moreover, the electrochemical nature of **1** and **2** was explored by means of three-electrode system using 1 mM $K_4[Fe(CN)_6]$ in 0.1 M KCl as supporting electrolyte. Previously electrochemical behavior of $\{P_2Mo_5\}$ cluster-based solids has been investigated only in acidic medium.[30,31] This is the first attempt to examine the nature of $\{P_2Mo_5\}$ cluster-based solids when $K_4[Fe(CN)_6]$ is used in KCl as supporting electrolyte.

2. Experimental

2.1 *Synthesis and initial characterization*

0.4 g of $Na_2MoO_4\cdot 2H_2O$ (1.65 mmol, Merck) was dissolved in 20 mL of distilled water and labeled as Solution A. Solution B was prepared by dissolving 0.15 mL of 2-amino-3-methylpyridine (1.47 mmol, Aldrich) in 20 mL of distilled water. Subsequently, Solution B was slowing added to Solution A and kept under stirring for five minutes. Upon stirring a turbid solution was obtained. Thereafter, 1 M orthophosphoric acid (H_3PO_4, Merck, 85%) was added dropwise to obtain a clear solution (pH ∼ 1) and the resultant solution was left undisturbed for crystallization. After two weeks, needle-shaped crystals of **1** were obtained (Yield: 65-70% based on molybdenum). The crystals were washed with distilled water and acetone and allowed to dry at room temperature. The same procedure was repeated using 2-amino-4-methylpyridine instead of 2-amino-3-methylpyridine and block-shaped crystals of **2** were obtained (Yield: 65-70% based on molybdenum).

Elemental analyses (C, H and N) were performed on ELEMENTAR Vario EL III CHNS Analyzer. Results of CHN analysis of the bulk product were found to be consistent with the stoichiometry. Anal. Found: C, 24.78; H, 3.09; N, 9.70%: Calcd: C, 24.73; H, 3.16; N, 9.61% for **1** and C, 23.06; H, 3.63; N, 8.86%: Calcd: C, 23.02; H, 3.70; N, 8.95% for **2**. Fourier transform infrared (FTIR) spectra were recorded on KBr pellets using Shimadzu FTIR spectrophotometer (model: IR Affinity). FTIR spectra of **1** and **2** showed bands in the region 650-690, 750-830 and 900-930 cm^{-1} which are characteristic of molybdenum oxygen stretching. Bands at 1000-1100, 1400-1420 and 1620-1640 cm^{-1} were assigned to P-O stretching, N-H bending and C-H bending vibrations respectively.[32] In addition, FTIR spectrum of **2** showed bands at 3100-3400 cm^{-1} which could be attributed to O-H stretching (Figure S1, Supplementary Information). The bands for **1**: 3185 cm^{-1} – ν_{as} (N-H), 3083 cm^{-1} – ν_{as} (C-H), 2949 cm^{-1} – ν_s (C-H), 1655 cm^{-1} – δ_{as} (N-H), 1554 cm^{-1} – δ_s (N-H), 1455 cm^{-1} – δ_{as} (C-H), 1383 cm^{-1} – δ_s (C-H), 1233 cm^{-1} – ν_{as} (C-N), 1183 cm^{-1} – ν_s (C-N), 1068 cm^{-1}, 1028 cm^{-1} – ν (P-O), 926 cm^{-1} – ν (Mo-$O_{terminal}$), 668 cm^{-1}, 575 cm^{-1} – (Mo-$O_{bridging}$); for **2**: 3413 cm^{-1} – ν_s (OH), 3191 cm^{-1} – ν_{as} (N-H), 3086 cm^{-1} – ν_{as} (C-H), 2940 cm^{-1} – ν_s (C-H), 1300 cm^{-1} – δ (O-H), 1660 cm^{-1} – δ_{as} (N-H), 1536 cm^{-1} – δ_s (N-H), 1487 cm^{-1} – δ_{as} (C-H), 1370 cm^{-1} – δ_s (C-H), 1239 cm^{-1} – ν_{as} (C-N), 1182 cm^{-1} - ν_s (C-N), 1081 cm^{-1}, 1024 cm^{-1} – ν (P-O), 969 cm^{-1}, 882 cm^{-1} – ν (Mo-$O_{terminal}$), 654 cm^{-1}, 577 cm^{-1} – (Mo-$O_{bridging}$).

2.2 *X-ray crystallographic studies*

X-ray diffraction studies of crystal mounted on a capillary were carried out on a BRUKER AXS SMART-APEX diffractometer with a CCD area detector (MoKα = 0.71073 Å, monochromator: graphite).[33] Frames were collected at T = 293 K (for **1**) and 296 K (for **2**) by ω, ϕ and 2θ-rotation at 10 s per frame with SAINT.[34] The measured intensities were reduced to F^2 and corrected for absorption with SADABS.[34] Structure solution, refinement, and data output were carried out with the SHELXTL program.[35] Non-hydrogen atoms were refined anisotropically. C-H and N-H hydrogen atoms were placed in geometrically calculated positions by using a riding model. Images were created with the DIAMOND program.[36] Hydrogen bonding interactions in the crystal lattice were calculated with SHELXTL and DIAMOND.[35,36] Crystal and refinement data are summarized in Table 1.

2.3 *Other physical measurements*

Powder X-ray diffraction (PXRD) data was collected on a Malvern Panalytical Aeris diffractometer using Ni-filtered CuKα radiation. Data were collected with a step size of 0.02° and count time of 2s per step over the range $5° < 2\theta < 60°$. Thermogravimetric analysis (TGA) was done on Perkin-Elmer TGA7 from room temperature to 900 °C at a heating rate of 10 °C/min. in a nitrogen atmosphere to determine water and organic content as well as the overall thermal stability of the product. Scanning electron microscopic (SEM) studies were carried out on crystals mounted on carbon tape using FEI FESEM Quanta 200 at

Table 1. Crystallographic details for **1** and **2**.

	1	**2**
Formula	$C_{30}H_{45}Mo_5N_{10}O_{23}P_2$	$C_{30}H_{45}Mo_5N_{10}O_{29}P_2$
Formula weight	1455.40	1551.4
T (K)	293(2)	296(2)
Space Group	$P2_1/c$	*P -1*
a, Å	8.394(1)	11.728(1)
b, Å	27.398(6)	14.234(1)
c, Å	21.521(4)	19.589(1)
α, °	90.00	68.906(3)
β, °	97.68(3)	89.454(3)
γ, °	90.00	66.559(3)
V, Å^3	4905.1(18)	2765.1(4)
Z	4	2
d_{calc}, g·cm^{-3}	1.971	1.863
$\mu_{MoK\alpha}$, cm^{-1}	1.397	1.254
λ (Å)	0.71073	0.71073
$R_1(I > 2\sigma I)$, WR_2(all)	0.0408, 0.1114	0.0391, 0.1153
GOF	1.080	1.111
Largest difference map hole and peak (eÅ^{-3})	−1.35 and 0.88	−1.23 and 2.87
CCDC No.	1999772	1999773

an accelerating voltage of 20 kV. The electrochemical measurements were carried out on CH1608 electrochemical work station using a three-electrode system with saturated Ag/AgCl as the reference electrode and Platinum wire as a counter electrode. The working electrode was fabricated by coating solids **1** and **2** separately on glassy carbon electrode (GCE) by simple drop-casting method. 1 mM $K_4[Fe(CN)_6]$ in 0.1 M KCl was used as the supporting electrolyte to study the electrochemical properties.

3. Results and Discussion

3.1 *Crystal structure of **1** and **2***

The solids **1** and **2** are based on $\{P_2Mo_5\}$ cluster anion which consists of edge and corner-sharing MoO_6 octahedra forming a Mo_5O_{15} ring capped by two PO_4 tetrahedra; the anion is identical to the one found in many solids.[28] The crystal structure of $\{H\text{-}2a3mp\}_5[\{PO_3(OH)\}\{PO_4\}Mo_5O_{15}]$, **1** and $\{H\text{-}2a4mp\}_5[\{PO_3(OH)\}\{PO_4\}Mo_5O_{15}]\cdot 6H_2O$, **2** suggests the presence of one cluster anion and five monoprotonated ligand moieties per asymmetric unit (Figure 1). In addition, six lattice water molecules per asymmetric unit are present in **2**. Bond valence sum (BVS) calculations[37] indicate that in both **1** and **2**, one of the phosphate groups per cluster anion is protonated (henceforth referred to as $\{HP_2Mo_5\}$). Moreover, in both **1** and **2**, $\{HP_2Mo_5\}$ cluster anion exhibits extensive H-bonding interactions with ligand moieties; however, the nature of supramolecular interactions in **1** and **2** is quite different.

In **1**, protonation of terminal oxygen i.e., O22 on the phosphate group results in a strong H-bonding interaction (2.411(12) Å) between P=O and P-OH groups of neighboring clusters thereby dictating the formation of 1-D chains of $\{HP_2Mo_5\}$ cluster anions as shown in Figure 2a. While, four of the $\{H\text{-}2a3mp\}^+$ moieties *viz.,* {N3N4}, {N5N6}, {N7N8} and {N9N10} are connected to $\{HP_2Mo_5\}$ cluster anion through NH…O interactions; the fifth $\{H\text{-}2a3mp\}^+$ moiety i.e., {N1N2} also links the adjacent $\{HP_2Mo_5\}$ cluster anions through CH…O interactions to form 1-D chains (Figure 2b). H-bonding interactions in **1** have been summarized in Table S1 (Supplementary Information). The 1-D chains are further linked *via* {N9N10} moieties through H-bonding (N9H9C…O8: 2.324(24) Å) interaction to form 2-D zig-zag sheet. The formation of 2-D sheets is also reinforced by π…π interactions (3.551(5) Å) mediated by {N7N8} and {N9N10} moieties of neighboring 1-D chains (Figure 2c). The packing of 2-D sheets is facilitated by CH…π interactions as shown in Figure S2 (Supplementary Information). It is noteworthy that the structure showed solvent-accessible voids of diameter 3.8 nm (Figure S2c, Supplementary Information).

The crystal structure analysis of **2** suggests the formation of a dimeric unit of $\{HP_2Mo_5\}$ cluster anions linked *via* H-bonding interaction mediated by {N7N8} moiety. {N1N2}, {N3N4} and {N5N6}

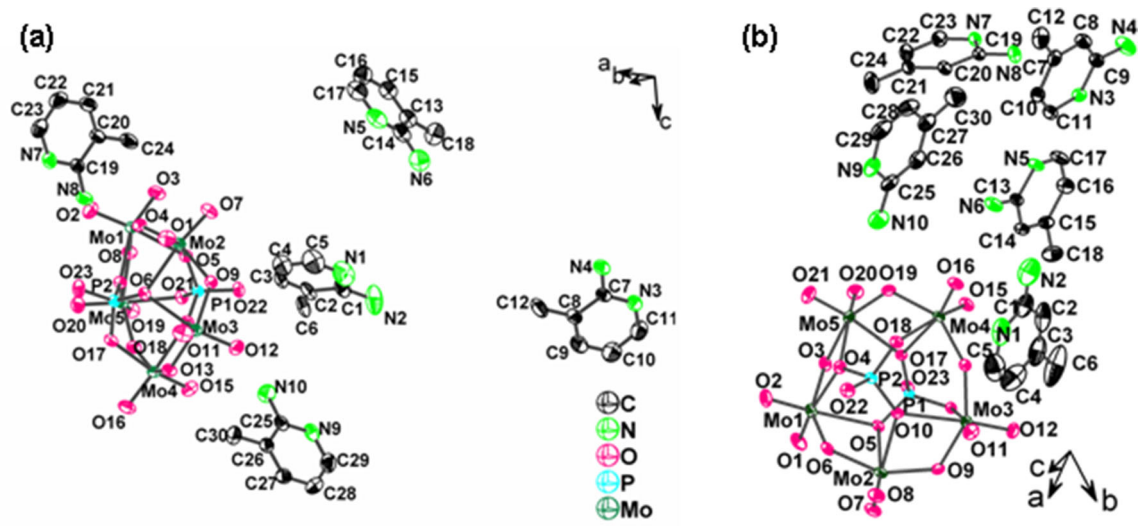

Figure 1. An ORTEP view of (a) **1** and (b) **2**. The lattice water molecules in **2** have been removed for clarity.

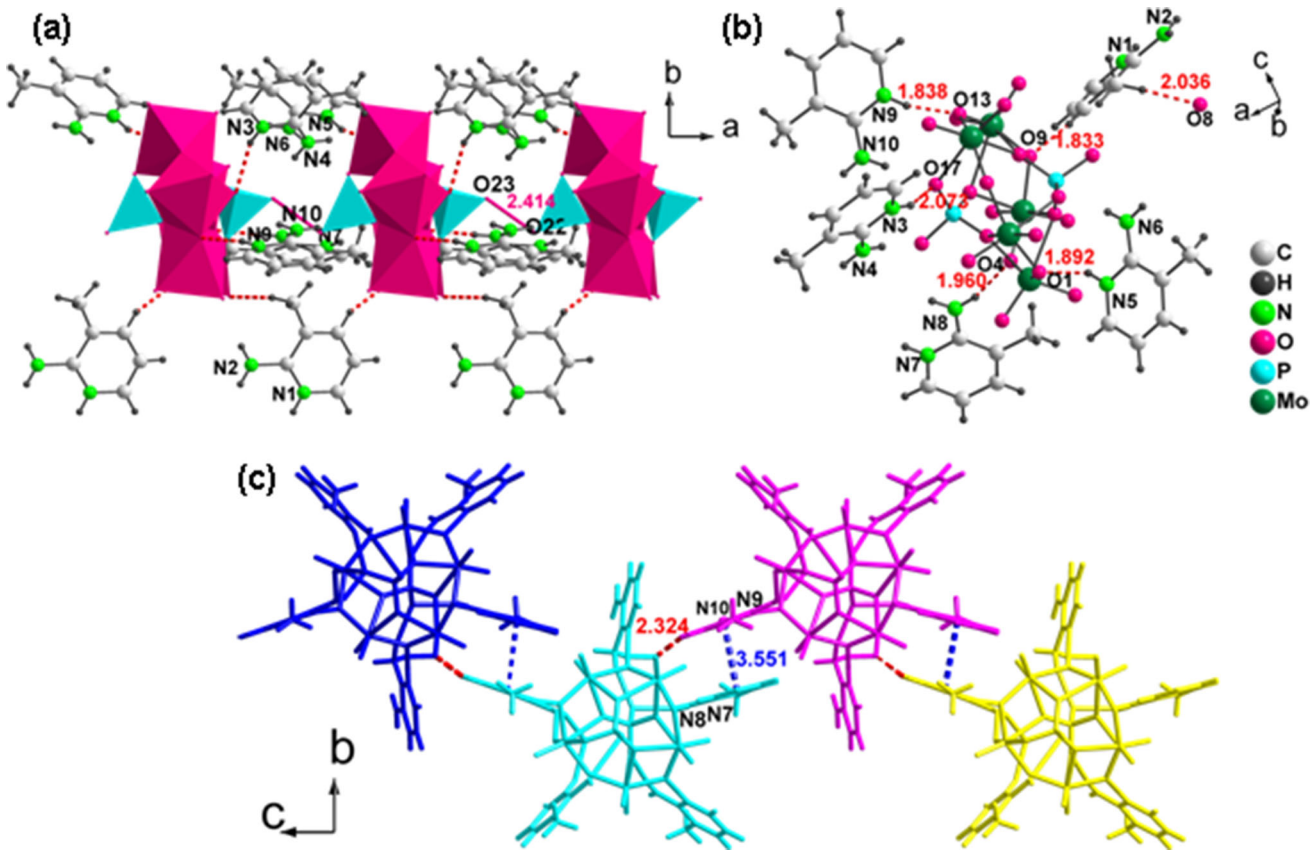

Figure 2. (a) 1-D chains in **1** mediated by O…O interactions (shown in solid red lines) between terminal oxygen atoms O22 and O23 of phosphate groups of neighboring cluster anions. Formation of 1-D chains is also facilitated by CH…O interactions (shown in dashed red lines) mediated by {N1N2} moieties. (b) H-bonding interactions exhibited by $\{HP_2Mo_5\}$ cluster anion in **1**. (c) Formation of the zig-zag 2-D sheet through CH…O and π…π interactions (shown in dashed red and blue lines, respectively) between neighboring 1-D chains. Four such chains are shown in blue, cyan, purple and yellow.

moieties along with five lattice water molecules are attached to the dimeric unit through NH…O and O…O interactions, respectively (Tables S2 and S3, Supplementary Information for H-bonding and O…O interactions). Each of the dimers is further connected through pentameric water cluster to form 1-D chains

which propagate along *b* axis as shown in Figure 3c. The packing resulted in voids which are occupied by {N9N10} moieties. The occurrence of {N9N10} moieties in the voids is induced by the pentameric water cluster through O6W (N10H10A…O6W: 2.131(6) Å). Inter-chain H-bonding interaction mediated by {N5N6} moiety (N6H6B…O16: 2.127(5) Å) results in 2-D sheet in *ab* plane. Unlike in **1**, CH…π interactions between neighboring chains facilitated the packing of 1-D chains in **2**. The 2-D sheets are stacked

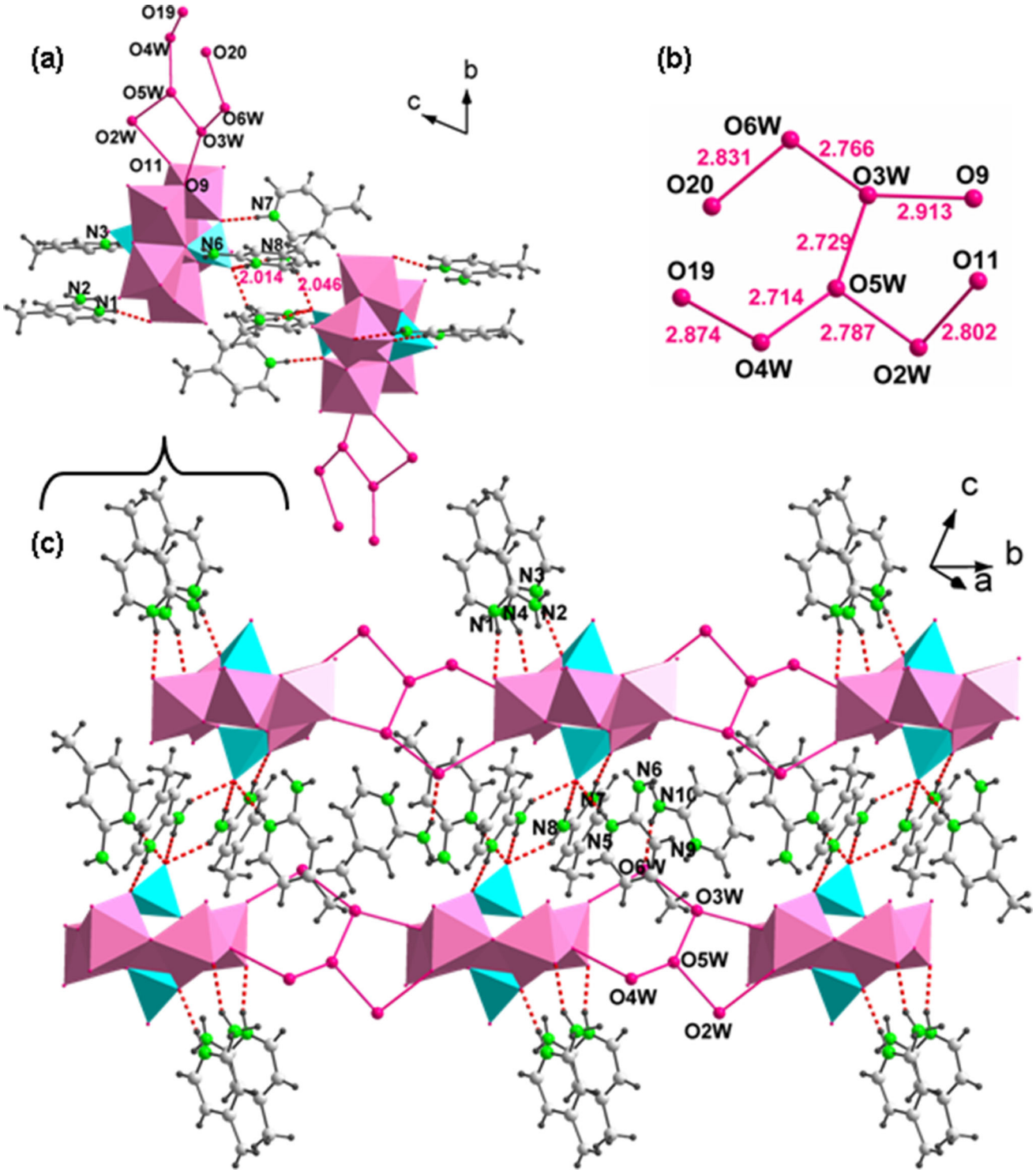

Figure 3. (a) Dimeric unit in **2** wherein $\{HP_2Mo_5\}$ cluster anions are linked through H-bonding (shown in dashed red lines) mediated by {N7N8} moiety. The pentameric water cluster is anchored to the dimer through O…O interactions shown in solid red lines. (b) The pentameric water cluster in **2**. (c) Dimer units linked through water clusters to form 1-D chain propagating along *b* axis. The 1-D chains result in voids which are occupied by {N9N10} moieties.

parallel to each other along the *c* axis through a lattice water molecule, O1W as shown in Figure S3, Supplementary Information.

3.2 *Analysis of solids **1** and **2***

SEM images of **1** and **2** showed the formation of well defined elongated needles and block-like morphology respectively (Figure 4). TG analysis of **1** and **2** (Figure S4, Supplementary Information) showed weight loss in two and three steps respectively. In **1**, the first weight loss upto 350 °C corresponding to 36.7% was due to the thermal degradation of five organic moieties. The second weight-loss upto 800 °C could be assigned to the decomposition of $\{HP_2Mo_5\}$ cluster anion. On the contrary, **2** showed an initial weight loss of 1.1% at 100 °C corresponding to the loss of one water molecule. The loss of remaining water molecules along with protonated organic moieties was observed at a slightly higher temperature (upto 350 °C), as water molecules formed a pentameric water cluster in **2**. The third weight loss could be attributed to the decomposition of $\{HP_2Mo_5\}$ cluster anion.

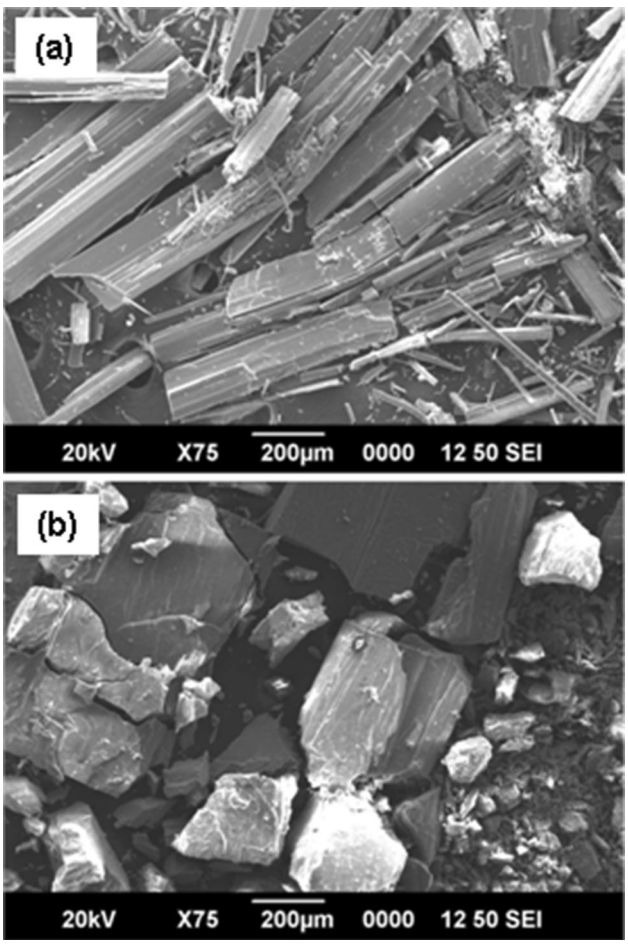

Figure 4. SEM images of (a) **1** and (b) **2**.

In both **1** and **2**, the phase purity of the solids was established by comparing the experimental PXRD pattern with simulated powder pattern of the single-crystal structure as shown in Figures S5-S6, Supplementary Information.

3.3 *Electrochemical behavior*

The redox behavior of the solids was investigated using cyclic voltammetry in 1 mM $K_4[Fe(CN)_6]$ with a scan rate of 50 mVs^{-1}. In both **1** and **2**, two reversible waves (I-I' & II-II') were observed in the potential range between −0.2 and +0.8 V (Figure 5a). The bare GCE gives a redox peak for $K_4[Fe(CN)_6]$ with mean peak potential E*1/2* = (*Eap* + *Epc*)/2 at 0.317 V which can be attributed to Fe^{II}/Fe^{III}.[38] The oxidation-reduction couple I-I' (+0.275 V and +0.279 V for **1** and **2**, respectively) could be attributed to potassium ferrocyanide which shows a shift towards negative potential. The redox peak II-II' in **1** and **2** with half-wave potentials +0.087 V and +0.072 V could be attributed to Mo^{VI}/Mo^{V} electron process. The slight deviations in the values can be ascribed to the different structural environment of $\{HP_2Mo_5\}$ clusters. The responses at +0.087 V and +0.072 V for solids **1** and **2** corresponding to Mo^{VI}/Mo^{V} electron process of the Strandberg cluster was further confirmed by comparing the cyclic voltammogram of the solid with that of the organic ligand used in its synthesis. For example, 2-amino-4-methylpyridine (2*a*4*mp*) is the organic ligand used for the synthesis of **2**. The value of E*1/2* = + 0.275 V was observed for 2*a*4*mp* which is quite distinct from the redox peaks detected for solid **2** corresponding to Fe^{II}/Fe^{III} and Mo^{VI}/Mo^{V} processes (Figure 5b).

3.4 *Chemistry of formation*

Solvent evaporation technique is one of the most facile methods employed for the crystallization of hybrid solids. The synthetic methodology used in the current study involves the mixing of aqueous molybdate solution with organic ligand under constant stirring. However, mixing of the two solutions results in immediate precipitation of an amorphous solid. Therefore the solution is acidified using H_3PO_4 to obtain a clear solution. The latter when left undisturbed results in crystallization of solids **1** and **2**. The

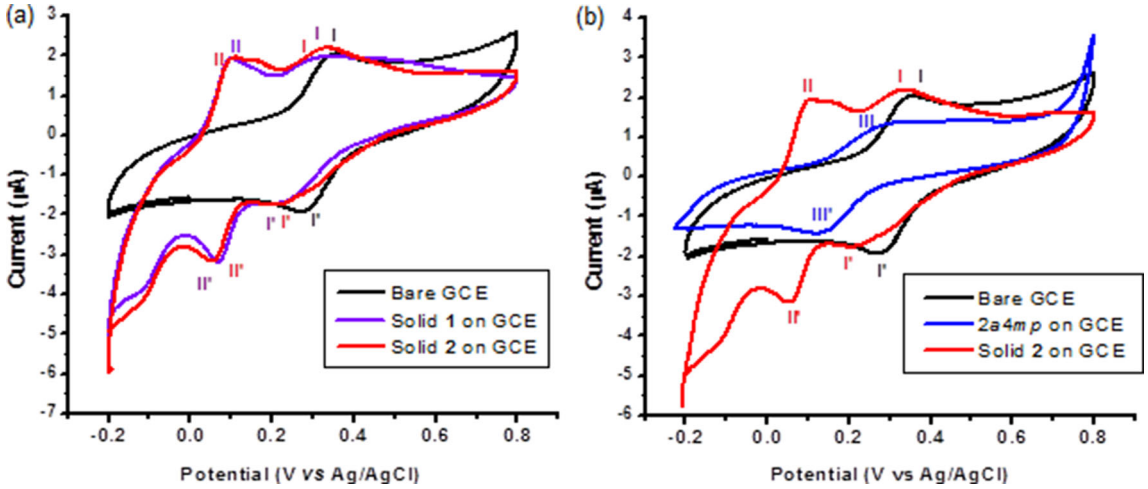

Figure 5. (a) Cyclic voltammogram for **1** and **2** in the presence of 1 mM $K_4[Fe(CN)_6]$ in 0.1 M KCl with a scan rate of 50 mVs^{-1}. (b) Comparison of voltammogram of 2*a*4*mp* with bare GCE and Solid **2**.

addition of H_3PO_4 has a two-fold effect. Firstly, it acts as a source of phosphate ions. Hence crystallization of PMO cluster-based solids is facilitated. Secondly, the pH of the reaction medium is adjusted to ~1. The highly acidic pH favors the formation of $\{HP_2Mo_5\}$ cluster anion[25] and results in protonation of the organic ligands (L). The formation of the solids can be visualized using the following equations wherein the Strandberg type polyoxometalate cluster is formed by protonation of tetrahedral molybdate; which under highly acidic conditions undergoes protonation:

$$5[MoO_4]^{2-} + 2\,PO_4^{3-} + 10H^+ \rightarrow \left[\{PO_4\}_2Mo_5O_{15}\right]^{6-} + 5H_2O$$

$$\left[\{PO_4\}_2\,Mo_5O_{15}\right]^{6-} + H^+ \rightarrow \left[\{PO_3(OH)\}\{PO_4\}Mo_5O_{15}\right]^{5-}$$

Initially, an electrostatic attraction between negativity charged $\{HP_2Mo_5\}$ cluster anion and positively charged organic moieties $(HL)^+$ initiates the self-assembly of solids **1** and **2**. The supramolecular assembly is further supported by secondary interactions which play a crucial role in crystal packing of these solids. Both the ligands have readily available $–NH_2$ and –NH groups which induce H-bonding interactions between the cluster anions and $(HL)^+$ units. The presence of the aromatic ring in organic moieties ensures the possibility for π …π and CH…π interactions between $(HL)^+$ counter ions.[39,40] Therefore, the role of H-bonding, π …π and CH…π interactions in crystal packing in **1** and **2** seems obvious.

Additionally, the crystal structure of **2** also showed the presence of lattice water molecules. Earlier we have demonstrated in several examples that aggregation of water cluster is a secondary factor in the crystal packing of such complex structures.[27] Protonation of Strandberg-type cluster anion[1] and synthesis under ambient conditions[25] are the key factors responsible for the aggregation of water molecules in PMO cluster-based solids. Strikingly, of the two solids, only **2** favored the formation of a pentameric water cluster. This could be attributed to the directionality of substituents on the organic ligands. While the hydrophobic methyl group is in close proximity to the amino group in 2*a*3*mp*, the comparatively distant position of methyl group in 2*a*4*mp* allows $–NH_2$ group to form H-bond with lattice water molecules in **2**. Therefore, aggregation of water cluster is induced in **2**.

4. Conclusions

Two new Strandberg-type cluster based solids *viz.*, $\{H\text{-}2a3mp\}_5[\{PO_3(OH)\}\{PO_4\}Mo_5O_{15}]$, **1** and $\{H\text{-}2a4mp\}_5[\{PO_3(OH)\}\{PO_4\}Mo_5O_{15}]\cdot 6H_2O$, **2** were successfully synthesized and characterized. Detailed structural analysis revealed the role of supramolecular interactions in the crystal packing of these solids. In addition, the formation of pentameric water cluster in **2** was rationalized on the basis of supramolecular interactions and directionality of substituents on the organic ligands. Further, the electrochemical nature of **1** and **2** was explored by means of a three-electrode system using 1 mM $K_4[Fe(CN)_6]$ in 0.1 M KCl as supporting electrolyte. To the best of our knowledge, the redox behavior of $\{P_2Mo_5\}$ cluster-based solids in the presence of $K_4[Fe(CN)_6]$ has not been examined so far. Cyclic voltammogram of both **1** and **2** showed reversible waves corresponding to Mo^{VI}/Mo^{V} electron process. The facile synthetic methodology used for the preparation of solids **1** and **2** can be successfully

applied for the crystallization of new hybrid solids based on Strandberg-type cluster anion. Moreover, a careful selection of the organic counterpart can modify electrochemical behavior along with porosity in hybrid solids.

Supplementary Information (SI)

CCDC 1999772 and 1999773 contain the supplementary crystallographic data for **1** and **2**. The data can be obtained freely via http://www.ccdc.cam.ac.uk/data_request/cif, or by e-mailing to data_request@ccdc.cam.ac.uk or by contacting directly the Cambridge Crystallographic Data Centre (12 Union Road, Cambridge CB2 1EZ, UK. Fax: +44 1223 336033). Tables of H-bonding and O…O interaction; FTIR spectra, figures showing CH…..π and π…..π interactions, TGA curves, figures showing the comparison of simulated and experimental PXRD patterns are available as supplementary information at www.ias.ac.in/chemsci.

Acknowledgements

JT thanks UGC for research project 2243-MRP/15-16/KLCA019/UGC-SWRO. The authors acknowledge DST and UGC for FIST and CPE program respectively implemented in St. Thomas College (Autonomous), Thrissur. The authors wish to thank Department of Chemistry, IIT Delhi for providing smart apex CCD single-crystal X-ray diffractometer under FIST for collecting data of Solid **1**. The authors also acknowledge Sophisticated Test and Instrumentation Centre (STIC), Cochin University for availing Single crystal XRD facility for collecting data of Solid **2**, scanning electron microscopy, CHN analyses and thermogravimetric analysis.

References

1. Upreti S and Ramanan A 2006 Role of hydrogen-bonded interactions in the crystal packing of phenylenediammonium phosphomolybdates *Cryst. Growth Des.* **6** 2066
2. Shi S, Chen L, Zhao X, Ren B, Cui X and Zhang J 2018 Role of H-bonds in the crystal packing of three novel Strandberg-type polyoxoanion compounds *Inorg. Chim. Acta* **482** 870
3. Pathan S and Patel A 2014 Keggin type transition metal substituted phosphomolybdates: Heterogeneous catalysts for selective aerobic oxidation of alcohols and alkenes under solvent free condition *Catal. Sci. Technol.* **4** 648
4. Li C, Mizuno N, Yamaguchi K and Suzuki K 2019 Self-assembly of anionic polyoxometalate–organic architectures based on lacunary phosphomolybdates and pyridyl ligands *J. Am. Chem. Soc.* **141** 7687
5. Xun S, Guo T, He M, Ma R, Zhang M, Zhu W and Li H 2019 Magnetic mesoporous nanospheres supported phosphomolybdate-based ionic liquid for aerobic oxidative desulfurization of fuel *J. Colloid Interface Sci.* **534** 239
6. Joseph J, Radhakrishnan R C, Johnson J K, Joy S P and Thomas J 2020 Ion-exchange mediated removal of cationic dye-stuffs from water using ammonium phosphomolybdate *Mater. Chem. Phys.* **242** 122488
7. Abu-Zied B M, Farrag A A A and Asiri A M 2013 Preparation of caesium-substituted phosphomolybdic acid via solid-state ion exchange method *Powder Technol*. **246** 643
8. Lu L and Xie Y 2018 Phosphomolybdic acid cluster bridging carbon dots and polyaniline nanofibers *J. Mater. Sci*. **54** 4842
9. Manivel A and Anandan S 2011 Silver nanoparticles embedded phosphomolybdate–polyaniline hybrid electrode for electrocatalytic reduction of H_2O_2 *J. Solid State Electrochem.* **15** 153
10. Liu J, Wang J, Chen M and Qian D 2017 Fabrication, electrochemical and catalytic properties of the nanocomposites composed of phosphomolybdic acid and viologen-functionalized multi-walled carbon nanotubes *J. Nanopart. Res.* **19** 264
11. Niu J, Ma J, Zhao J, Ma P and Wang J 2011 A new 2D network polyoxometalate constructed from Strandberg-type phosphomolybdates linked through binuclear Ca(II) clusters *Inorg. Chem. Commun*. **14** 474
12. Ma X, Zhou F, Yue H, Hua J and Ma P 2019 A nanolinear zinc-substituted phosphomolybdate with reactive oxygen species catalytic ability and antibacterial activity *J. Mol. Struct*. **1198** 126865
13. Li Z L, Wang L C, Wang J P, You W S and Zhu Z M 2014 Three molybdophosphates based on Strandberg-type anions and Zn (II) - H_2biim/H_2O subunits: Synthesis, structures and catalytic properties *Dalton Trans*. **43** 5840
14. Strandberg R 1973 The molecular and crystal structure of $Na_6Mo_5P_2O_{23}(H_2O)_{13}$ a compound containing sodium-coordinated pentamolybdodiphosphate anions *Acta Chem. Scand*. **27** 1004
15. Shi Z, Li F, Zhao J, Yu Z Y, Zheng Y, Chen Z, Guo Q, Zhang G and Luo Y 2019 A 3D inorganic-organic hybrid constructed from Strandberg-type polyoxometalates and silver complexes: Synthesis, structure and properties *Inorg. Chem. Commun.* **102** 104
16. Ji Y M, Zhao M, Han P P, Fang Y, Han Q X and Li M X 2018 Cobalt (II) compound derived from Strandberg-type polyoxometalate clusters: Synthesis, crystal structures and biological activities *Inorg. Nano-Met. Chem*. **48** 421
17. Xu M, Li F, Wang T and Xu L 2018 Single ion sandwich-type polyoxomolybdates based on Strandberg anions and their electrocatalytic properties *Inorg. Chem. Commun*. **94** 123
18. Zhao H, Li J, Fang Y, Chang B, Meng Q, Li M, Wang C and Zhu X 2020 Synthesis, characterization and bioactivities of a new covalent copper (II) compound derived from $\{P_2Mo_5O_{23}\}^{6-}$ and thiosemicarbazones *Bioorg. Med. Chem. Lett*. **30** 126781
19. Ganesan S V and Natarajan S 2005 Hydrothermal synthesis and structure of $[(C_4N_2H_{12})_3][P_2Mo_5O_{23}]\cdot H_2O$ and $[(C_3N_2H_{12})_3][P_2Mo_5O_{23}]\cdot 4H_2O$ *J. Chem. Sci.* **117** 219

20. Upreti S and Ramanan A 2008 Water oligomers in the crystal engineering of phenylenediammonium diphosphopentamolybdates *Synth. React. Inorg. Metal-org. Nano-Metal Chem.* **38** 69
21. Asnani M, Kumar D, Duraisamy T and Ramanan A 2012 Crystallization of organically templated phosphomolybdate cluster-based solids from aqueous solution. *J. Chem. Sci.* **124** 1275
22. Ma F X, Chen Y G, Yang H Y, Dong X W, Jiang H, Wang F and Li J H 2019 The pH-controlled hydrothermal synthesis and crystal structure of two novel phosphomolybdate derivatives *J. Cluster. Sci*. **30** 123
23. Paul L, Dolai M, Panja A and Ali M 2016 Hydrothermal synthesis of two supramolecular inorganic-organic hybrid phosphomolybdates based on Ni (II) and Co) II) ions: Structural diversity and heterogeneous catalytic activities *New J. Chem.* **40** 6931
24. Qu M, Feng H, Ma C, Yang Y and Yu X 2017 Synthesis, crystal structure and anti-tumor activity of a novel 3D supramolecular compound constructed from Strandberg-type polyoxometalate and benzimidazole *Inorg. Chem. Commun*. **81** 22
25. Thomas J and Ramanan A 2008 Growth of copper pyrazole complex templated phosphomolybdates: Supramolecular interactions dictate nucleation of crystal *Cryst. Growth. Des*. **8** 3390
26. Thomas J and Ramanan A 2011 Phosphomolybdate cluster based solids mediated by transition metal complexes *Inorg. Chim. Acta* **372** 243
27. Thomas J, Kumar D and Ramanan A 2013 Crystallization of phosphomolybdate clusters mediated by copper azole complexes: Influence of pH and temperature *Inorg. Chim. Acta* **396** 126
28. Thomas J, Ph.D. Thesis, Indian Institute of Technology, Delhi, India, 2010
29. Zhai Q, Wu X, Chen S, Chen L and Lu C 2007 Keggin polyoxometalates – supported assembly of 2D supramolecular isomers: Synthesis, crystal structures and characteristics of two novel hybrid host–guest complexes *Inorg. Chim. Acta* **360** 3484
30. Harchani A and Haddad A 2015 Synthesis, structure and property of a new diphosphopentamolybdates $[C_7H_7N_2]_2[H_2P_2Mo_5O_{23}]_{0.5}.3.5H_2O$ *J. Clust. Sci*. **26** 1645
31. Song L, Yu K, Su Z, Wang C, Wang C and Zhou B 2014 Assembly of three supramolecular compounds based on $[P_2Mo_5O_{23}]^{6-}$ and Ni (II) complexes *J. Coord. Chem.* **67** 522
32. Nakamoto K 1978 *Infrared and Raman Spectra of Inorganic and Coordination Compounds* (New York: John Wiley & Sons)
33. Bruker Analytical X-ray Systems, SMART: Bruker Molecular Analysis Research Tool, Version 5.618, 2000
34. Bruker Analytical X-ray Systems, SAINT-NT, Version 6.04, 2001
35. Bruker Analytical X-ray Systems, SHELXTL-NT, Version 6.10, 2000
36. Klaus B., University of Bonn, Germany DIAMOND, Version 4.1
37. Brown I D and Altermatt D 1985 Bond-valence parameters obtained from a systematic analysis of the Inorganic Crystal Structure Database *Acta Crystallogr*. **B41** 244
38. Jose J, Rajamani A R, Anandaram S, Jose S P, Peter S C and Sreeja P B 2019 Photophysical and electrochemical studies of anchored chromium (III) complex on reduced graphene oxide via diazonium chemistry *Appl. Organomet. Chem*. e5063
39. Desiraju G R, Vittal J J and Ramanan A 2011 *Crystal Engineering—A Textbook* (Singapore: World Scientific Publishing)
40. Das D and Biradha K 2019 Cocrystals and salts of 3,5-bis(pyridinylmethylene)-piperidin-4-one with aromatic poly-carboxylates and resorcinols: influence of stacking interactions on solid-state luminescence properties *Austr. J. Chem.* **72** 742